

Selective Electrocatalytic Reduction of Nitrous Oxide to Dinitrogen with an Iron Porphyrin Complex

Jared S. Stanley, Xinran S. Wang, Jenny Y. Yang*

Department of Chemistry, University of California, Irvine, Irvine, CA 92697, USA

ABSTRACT: Nitrous oxide (N₂O) is the third largest contributor to anthropogenic greenhouse gas emissions and plays a detrimental role in the depletion of ozone. Despite the contribution of N₂O as an atmospheric pollutant, there are currently only a few examples of electrochemical N₂O remediation to N₂. Herein we report the electrocatalytic deoxygenation of N₂O by iron tetraphenylporphyrin (FeTPP) to form N₂ with quantitative Faradaic efficiency and an observed rate of 12.6 s⁻¹. Comprehensive mechanistic investigation of the proposed steps in the catalytic cycle determined that hydrogen-bond donors are critical for accelerating N₂O activation and that proton transfer is involved in the rate-determining step.

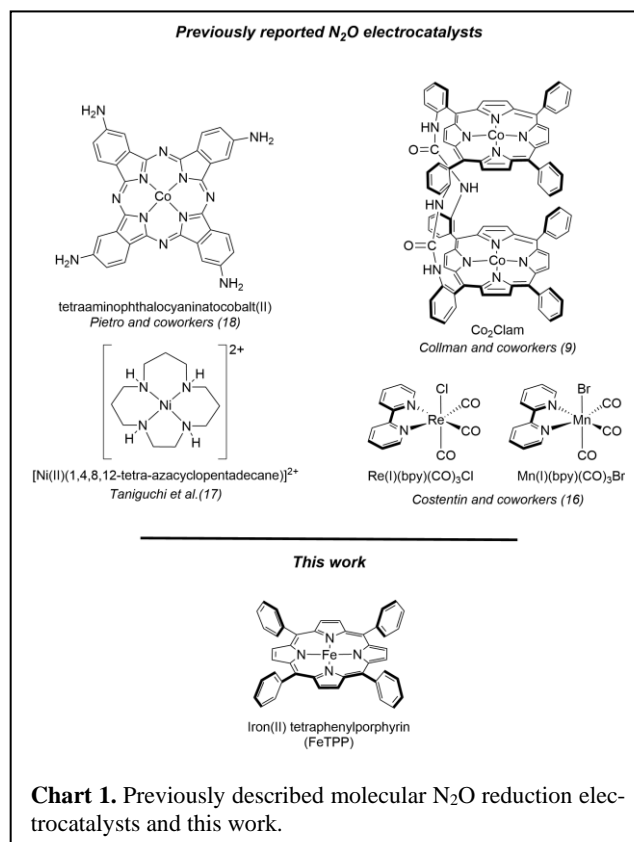
Coined as “laughing gas,” nitrous oxide (N₂O) has been employed in a variety of applications, ranging from its use as an anesthetic to an additive in rocket fuel.^{1,2} Recently, the anthropogenic emission of N₂O has been rising due to industrial processes and excess fertilizer use in agriculture.^{3,4} As a result, atmospheric N₂O concentration is increasing by approximately 0.75 ppb yearly.⁵ Consequently, N₂O has been identified as the leading contributor to ozone depletion in the 21st century.⁶ N₂O is also estimated to have 300 times the global warming potential compared to CO₂ and a lifetime of ~114 years in the atmosphere.⁷ Thus, the remediation of N₂O into benign products is important for minimizing negative environmental effects from industrial and natural sources.

N₂O is a powerful oxidant, with a standard potential of +1.77 V vs. NHE for the reaction shown below.^{8,9}



However, N₂O is kinetically inert. Designing complexes for activation under ambient conditions has been a long-standing goal for several reasons, including remediation, application as a terminal oxidant, and understanding biological activity.¹⁰⁻¹³ Because it is so unreactive and a poor ligand, there are only a handful of examples of N₂O activation at homogeneous catalysts.^{4,14,15} There are even fewer examples of selective N₂O reduction electrocatalysts (Chart 1).¹⁶⁻¹⁸

We explored iron(II) tetraphenylporphyrin (FeTPP) for electrocatalytic activity towards N₂O reduction. FeTPP is oxidatively stable and commercially available as the precatalyst iron(III) tetraphenylporphyrin chloride (FeTPP-Cl). Iron porphyrin derivatives have previously displayed reactivity with N₂O as an oxidant in the catalytic reductive dimerization of alkenes.¹⁹ Additionally, FeTPP has well characterized electrocatalytic activity towards the reduction of CO₂ to CO.^{20,21} As noted by Costentin and coworkers, there are several parallels between N₂O and CO₂ reduction. N₂O is isoelectronic to CO₂, and both molecules can react with two electrons and two protons to cleave the heteroatom-oxygen bond and form N₂ and CO, respectively. Both N₂O and CO₂ also contain a central electrophilic atom that can bind to an electron-rich metal center.¹⁶ Further, most prior examples of N₂O reduction catalysts have activity towards CO₂ to CO reduction. The combination of these



factors led us to investigate the electrocatalytic reduction of N₂O by FeTPP.²²

Consistent with prior reports, cyclic voltammetry (CV) of FeTPP-Cl (1 mM in THF) under 1 atm of Ar contains three reduction events (Figure 1, top, black).²³ The first event is the quasi-reversible reduction of Fe(III) to Fe(II) coupled with dissociation of the axial chloride ligand at -0.9 V vs Fe(C₅H₅)₂⁺⁰.²³ The next two reductions events are at -1.7 and -2.2 V vs Fe(C₅H₅)₂⁺⁰ and are centered on the porphyrin ligand to form the anion and dianion complex, respectively.²⁴

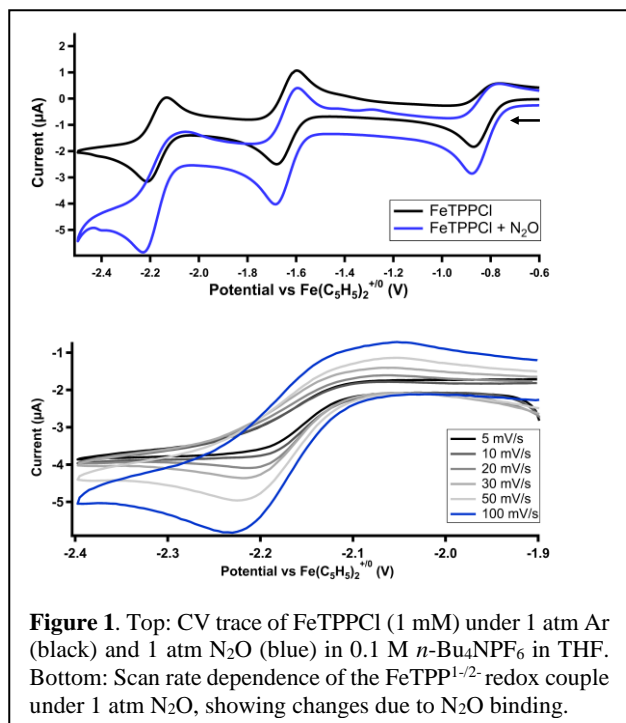


Figure 1. Top: CV trace of FeTPPcI (1 mM) under 1 atm Ar (black) and 1 atm N₂O (blue) in 0.1 M *n*-Bu₄NPF₆ in THF. Bottom: Scan rate dependence of the FeTPP^{1-/2-} redox couple under 1 atm N₂O, showing changes due to N₂O binding.

Under 1 atm of N₂O, the reduction feature at -2.2 V vs Fe(C₅H₅)₂⁺⁰ displays no corresponding anodic return peak at slow scan rates (less than 10 mV/s), indicating an EC mechanism, where E represents an electron transfer step and C represents a subsequent chemical step. (Figure 1 top, blue and Figure 1, bottom). The E represents the reduction to the fully reduced Fe(II)TPP²⁻ state, and we attribute the C step to N₂O binding to the metal center.

Titration of water into the FeTPPcI solution under 1 atm N₂O results in enhancement of the reductive current at -2.2 V vs Fe(C₅H₅)₂⁺⁰, indicating electrocatalytic activity (Figure 2). This current enhancement achieves a maximum value with approximately 21 equivalents of water (Figure 2). The relationship between the maximum catalytic current with water and N₂O, and the non-catalytic current can be used to calculate an observed pseudo-first-order rate constant in pure kinetic zones, where the cathodic current is not limited by diffusion of the substrate. This relationship is given by Equation 1,

$$\text{Equation 1.} \quad k_{obs} = \left[\frac{i_c}{i_p} \frac{0.446}{n} \right]^2 (n')^3 \frac{Fv}{RT}$$

where i_c is the peak catalytic current, i_p is the peak non-catalytic current, n is the number of moles consumed in a catalytic cycle, n' is the number of electrons consumed by the catalyst, and v is the scan rate (V/s).²⁵ Analysis of our data resulted in $k_{obs} = 12.6 \text{ s}^{-1}$.

Controlled potential electrolysis (CPE) of FeTPPcI (1 mM in 0.1 M *n*-Bu₄NPF₆ in THF) was performed with 20 equivalents of water under an atmosphere of N₂O to confirm catalytic turnover and quantify product formation. A potential of -2.3 V vs Fe(C₅H₅)₂⁺⁰ was applied for 2.2 hours, resulting in a linear variation of charge passed with time (Figure 3, blue). The headspace of the electrolysis cell was sampled using gas chromatography to determine the identity and the quantity of products formed. When catalyst was present, N₂ was quantified with an average Faradaic efficiency of 100 ± 5%. The amount of current

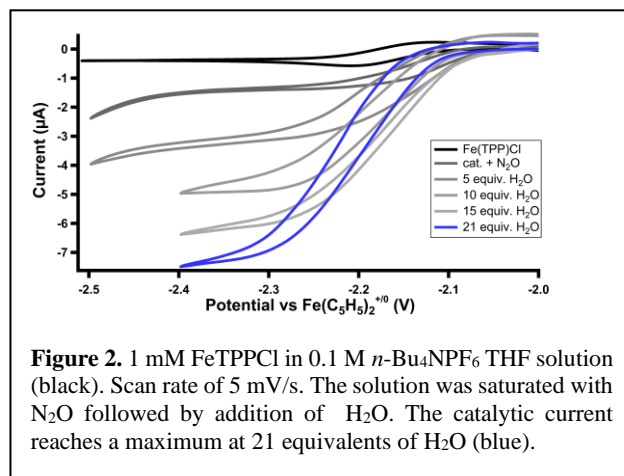


Figure 2. 1 mM FeTPPcI in 0.1 M *n*-Bu₄NPF₆ THF solution (black). Scan rate of 5 mV/s. The solution was saturated with N₂O followed by addition of H₂O. The catalytic current reaches a maximum at 21 equivalents of H₂O (blue).

passed is equivalent to 8.65 turnovers per catalyst. No H₂ was detected. No gaseous products were detected when no catalyst was present (Figure 3, black).

The proposed catalytic cycle is shown in Scheme 1. After three one-electron reductions of Fe(III)TPPcI, N₂O binds as indicated by the EC mechanism observed by cyclic voltammetry, with an electron transfer event followed by an irreversible chemical step. No loss of reversibility is observed under 1 atm Ar with H₂O present, providing further evidence that the initial reaction with the fully reduced complex is with N₂O and not H₂O. This intermediate then interacts with two equivalents of acid and two equivalents of electrons to cleave the heteroatom-oxygen bond and generate an equivalent of water, ending with dissociation of the reduced substrate. The proposed mechanism is also consistent with reported iron porphyrin CO₂ reduction systems, in which the iron porphyrin complex is first reduced to the doubly-reduced Fe(II)TPP, or Fe(II)TPP²⁻, before the substrate is bound.²⁶

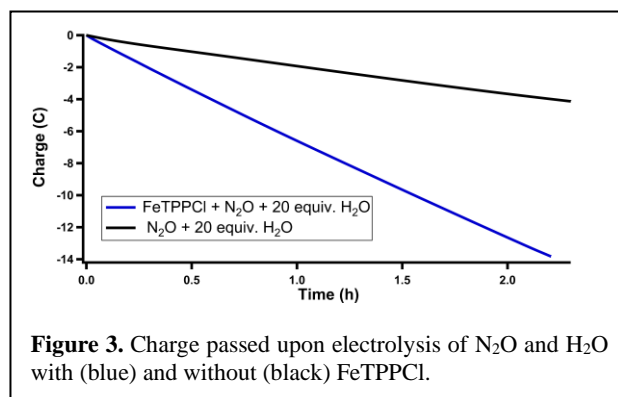
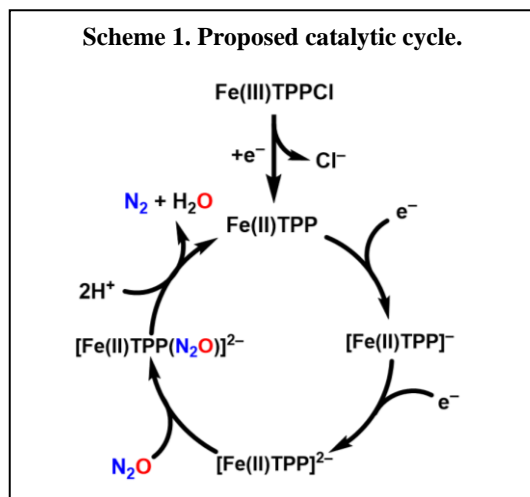


Figure 3. Charge passed upon electrolysis of N₂O and H₂O with (blue) and without (black) FeTPPcI.

Post-electrolysis ultraviolet-visible (UV-vis) absorption spectra of the solution indicate a new compound is formed. The N₂O-bound reduced iron complex was generated independently using *in situ* spectroelectrochemistry (Figure 4, S6 and S7). These spectra match that of the post electrolysis solution, indicating the resting state under catalytic conditions.

As the third reduction of Fe(III)TPPcI results in the initial reaction with N₂O and a loss of reversibility, this step was studied under non-catalytic conditions to determine the rate (k_{obs}) of N₂O binding. Scan rate dependent studies on this EC redox event under 1 atm N₂O in the absence of water were performed.



This data was analyzed by monitoring the ratio of anodic to cathodic current versus the scan rate as previously described by Savéant (Figures S1 & S2).²⁷ From this analysis, the pseudo-first-order rate for N₂O binding is $0.06 \text{ s}^{-1} < k_{obs} < 0.08 \text{ s}^{-1}$.²⁸ This rate is an order of magnitude faster than the reported k_{obs} for the analogue CoTPP, but slower than the binary “face-to-face” cobalt porphyrin systems.⁹

The rate for N₂O binding to Fe(II)TPP²⁻ is notably slower than the overall k_{obs} for catalysis (12.6 s^{-1}). However, no water is present during the rate measurement. We initially hypothesized that water could increase the N₂O binding rate through axial ligation to the Fe, increasing the electron density at the metal. However spectroelectrochemical analysis demonstrates no coordination of water to the complex upon reduction to Fe(II)TPP²⁻ (Figure S9).

We then considered the possibility that water could serve as a hydrogen-bond donor that stabilizes the N₂O-bound complex. As water also serves as the proton donor for catalysis, we are unable to isolate its effect in the N₂O binding step without further reactivity and catalysis. In order to deconvolute the impact of hydrogen-bonding on N₂O binding while inhibiting protonation and catalysis, we used the more basic secondary amine 2,2,6,6-tetramethylpiperidine (TMP). TMP is a hydrogen-bond donor, although its donor strength is expected to be weaker than H₂O.²⁵ However, it is also a much weaker Bronsted acid. Although its pK_a has not been measured in THF, its pK_a is 37 in DMSO, compared the pK_a of 32 for water.²⁹ Cyclic voltammetry of FeTPP·Cl under 1 atm N₂O and 60 mM TMP verifies minimal or no electrocatalytic activity (Figure S17) with this hydrogen-bond donor.

The rate of N₂O binding was evaluated using the same scan-rate dependent cyclic voltammetry analysis under 1 atm N₂O and 60 mM 2,2,6,6-tetramethylpiperidine. A significant increase in the observed rate constant was measured (6.7 s^{-1}) for N₂O binding (Figure S3). The increased rate constant with TMP suggests that the presence of a hydrogen-bond donor facilitates N₂O binding. While the measured rate for this step does not reach the electrocatalytic rate of 12.6 s^{-1} when H₂O is present, TMP is not as strong of an H-bond donor as water since oxygen is more electronegative than nitrogen.³⁰

To investigate the kinetic isotope effect, D₂O was used as the acid source instead of H₂O, where k_D was determined by the same method presented in Equation 1. The primary kinetic isotope effect observed ($k_H/k_D = 2.1$) indicates proton transfer is involved in the rate determining step (RDS). This RDS could

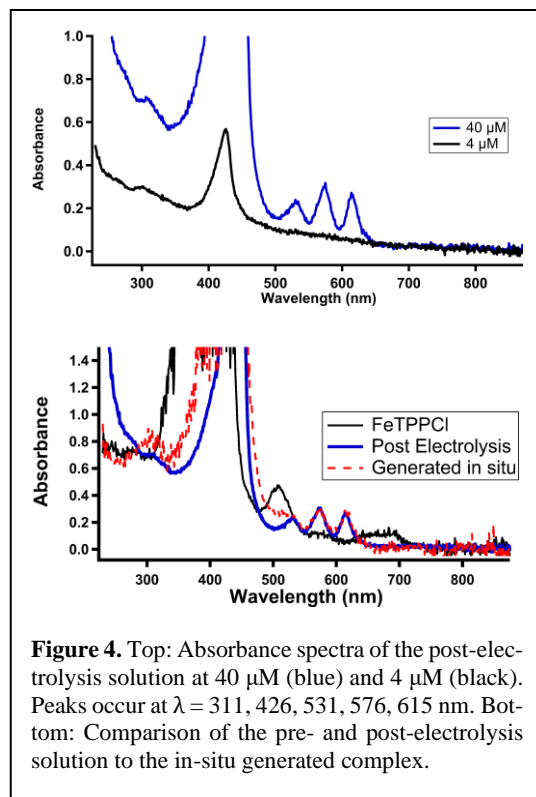


Figure 4. Top: Absorbance spectra of the post-electrolysis solution at 40 μM (blue) and 4 μM (black). Peaks occur at $\lambda = 311, 426, 531, 576, 615 \text{ nm}$. Bottom: Comparison of the pre- and post-electrolysis solution to the in-situ generated complex.

be proton transfer to N₂O concerted with electron transfer and N–O bond breaking, which is consistent with our observed resting state of N₂O bound to the FeTPP²⁻ species. Furthermore, this mechanism would be consistent with the rate determining step for CO₂ reduction to CO by iron porphyrins.³¹

In summary, our study describes the electrocatalytic cleavage of the N–O bond of nitrous oxide by an iron porphyrin system using water as a proton donor. FeTPP·Cl has high selectivity for conversion to N₂ with no concomitant reduction of H₂O to H₂. Our electrochemical analysis indicates that N₂O binding occurs at Fe(II)TPP²⁻, and that intermolecular hydrogen-bond donors accelerate the rate of binding. Additionally, the kinetic isotope effect on rate indicates proton transfer is involved in the rate-determining step. Both of these aspects indicate that N₂O reduction to N₂ has parallel mechanistic features compared to CO₂ reduction to CO. These similarities to CO₂ reduction will likely prove useful in the development of N₂O remediation catalysts. This conversion represents another application of a diverse catalyst, and an important step in the remediation of nitrous oxide.

ASSOCIATED CONTENT

Supporting Information. General, electrochemical, and physical methods, calculations, UV-visible spectroelectrochemical data, cyclic voltammograms. This material is available free of charge via the Internet at <http://pubs.acs.org>.

AUTHOR INFORMATION

Corresponding Author

*j.yang@uci.edu

Author Contributions

The manuscript was written through contributions of all authors. / All authors have given approval to the final version of the manuscript.

Funding Sources

JSS was supported by the Center for Closing the Carbon Cycle, an Energy Frontier Research Center funded by the U.S. Department of Energy, Office of Science, Basic Energy Sciences under Award Number DE-SC0023427. XSW was supported by the School of Physical Sciences Solutions that Scale Fellowship Program.

ACKNOWLEDGMENT

JSS acknowledges support by the Center for Closing the Carbon Cycle, an Energy Frontier Research Center funded by the U.S. Department of Energy, Office of Science, Basic Energy Sciences under Award Number DE-SC0023427. XSW was supported by the School of Physical Sciences Solutions that Scale Fellowship Program.

REFERENCES

- (1) Zafirova, Z.; Sheehan, C.; Hosseinian, L. Update on Nitrous Oxide and Its Use in Anesthesia Practice. *Best Pract. Res. Clin. Anaesthesiol.* **2018**, *32* (2), 113–123. <https://doi.org/10.1016/J.BPA.2018.06.003>.
- (2) Dyer, J.; Doran, E.; Dunn, Z.; Lohner, K.; Bayart, C.; Sadhwani, A.; Zilliac, G.; Cantwell, B.; Karabeyoglu, A. Design and Development of a 100 Km Nitrous Oxide/Paraffin Hybrid Rocket Vehicle. **2007**. <https://doi.org/10.2514/6.2007-5362>.
- (3) Thiemens, M. H.; Troglor, W. C. Nylon Production: An Unknown Source of Atmospheric Nitrous Oxide. *Science (1979)* **1991**, *4996* (251), 932–934. <https://doi.org/10.1126/SCIENCE.251.4996.932>.
- (4) Severin, K. Synthetic Chemistry with Nitrous Oxide. *Chem Soc Rev* **2015**, *44* (17), 6375–6386. <https://doi.org/10.1039/C5CS00339C>.
- (5) Fahey, D. W.; Doherty, S. J.; Hibbard, K. A.; Romanou, A.; Taylor, P. C.; Fahey, D. J. W.; Dokken, D. J.; Stewart, B. C.; Maycock, T. K. Physical Drivers of Climate Change. *Climate Science Special Report: Fourth National Climate Assessment* **2017**. <https://doi.org/10.7930/J0513WCR>.
- (6) Ravishankara, A. R.; Daniel, J. S.; Portmann, R. W. Nitrous Oxide (N₂O): The Dominant Ozone-Depleting Substance Emitted in the 21st Century. *Science (1979)* **2009**, *326* (5949), 123–125. <https://doi.org/10.1126/SCIENCE.1176985>
- (7) Rees, R. M. Global Nitrous Oxide Emissions: Sources and Opportunities for Mitigation. *ACS Symposium Series* **2011**, *1072*, 257–273. <https://doi.org/10.1021/BK-2011-1072.CH014>
- (8) Ortega-Lepe, I.; Sánchez, P.; Santos, L. L.; Lara, P.; Rendón, N.; López-Serrano, J.; Salazar-Pereda, V.; Lvarez, E. A.; Paneque, M.; Suárez, A. Catalytic Nitrous Oxide Reduction with H₂ Mediated by Pincer Ir Complexes. *Inorg. Chem.* **2022**, *2022*, 61. <https://doi.org/10.1021/ACS.INORGCHEM.2C02963>.
- (9) Collman, J. P.; Marrocco, M.; Elliott, C. M.; L'Her, M. Electrocatalysis of Nitrous Oxide Reduction. Comparison of Several Porphyrins and Binary “Face-to-Face” Porphyrins. *Journal of Electroanalytical Chemistry* **1981**, *124* (1–2), 113–131. [https://doi.org/10.1016/S0022-0728\(81\)80289-6](https://doi.org/10.1016/S0022-0728(81)80289-6).
- (10) Jolly, W. *The Inorganic Chemistry of Nitrogen*; Benjamin: New York, 1964.
- (11) Parmon, V. N.; Panov, G. I.; Uriarte, A.; Noskov, A. S. Nitrous Oxide in Oxidation Chemistry and Catalysis: Application and Production *Catalysis Today* **2005**, *100*, 115–131. <https://doi.org/10.1016/j.cattod.2004.12.012>.
- (12) Lehnert, N.; Dong, H. T.; Harland, J. B.; Hunt, A. P.; White, C. J. Reversing Nitrogen Fixation. *Nature Reviews Chemistry* **2018**, *278*–289. <https://doi.org/10.1038/s41570-018-0041-7>.
- (13) Tolman, W. B. Binding and Activation of N₂O at Transition-Metal Centers: Recent Mechanistic Insights. *Angewandte Chemie - International Edition.* **2010**, 1018–1024. <https://doi.org/10.1002/anie.200905364>.
- (14) Pang, Y.; Leutzsch, M.; Nöthling, N.; Cornella, J. Catalytic Activation of N₂O at a Low-Valent Bismuth Redox Platform. *J. Am. Chem. Soc.* **2020**, *142* (46), 19473–19479. <https://doi.org/10.1021/jacs.0c10092>.
- (15) Sinhababu, S.; Lakliang, Y.; Mankad, N. P. Recent Advances in Cooperative Activation of CO₂ and N₂O by Bimetallic Coordination Complexes or Binuclear Reaction Pathways. *Dalton Transactions* **2022**. <https://doi.org/10.1039/d2dt00210h>.
- (16) Deeba, R.; Molton, F.; Chardon-Noblat, S.; Costentin, C. Effective Homogeneous Catalysis of Electrochemical Reduction of Nitrous Oxide to Dinitrogen at Rhenium Carbonyl Catalysts. *ACS Catal.* **2021**, *11* (10), 6099–6103. <https://doi.org/10.1021/ACSCATAL.1C01197>
- (17) Taniguchi, I.; Shimpuku, T.; Yamashita, K.; Ohtaki, H. Electrocatalytic Reduction of Nitrous Oxide to Dinitrogen at a Mercury Electrode Using NiII Complexes of Macrocyclic Polyamines. *J. Chem. Soc., Chem. Commun.* **1990**, 915–917.
- (18) Zhang, J.; Tse, Y.-H.; Lever, A. B. P.; Pietro, W. J. Electrochemical Reduction of Nitrous Oxide (N₂O) Catalysed by Tetraaminophthalocyanatocobalt(II) Adsorbed on a Graphite Electrode in Aqueous Solution. *J. Porphyrins and Phthalocyanines* **1998**, *1*, 323–331. [https://doi.org/10.1002/\(SICI\)1099-1409\(199710\)1:4](https://doi.org/10.1002/(SICI)1099-1409(199710)1:4).
- (19) Saito, S.; Ohtake, H.; Umezawa, N.; Kobayashi, Y.; Kato, N.; Hirobe, M.; Higuchi, T. Nitrous Oxide Reduction-Coupled Alkene-Alkene Coupling Catalysed by Metalloporphyrins †. *Chem. Commun.* **2013**, *49*, 8979. <https://doi.org/10.1039/c3cc43912g>.
- (20) Hammouche, M.; Lexa, D.; Savéant, J. M.; Momenteau, M. Catalysis of the Electrochemical Reduction of Carbon Dioxide by Iron(“0”) Porphyrins. *Journal of Electroanalytical Chemistry* **1988**, *249* (1–2), 347–351. [https://doi.org/10.1016/0022-0728\(88\)80372-3](https://doi.org/10.1016/0022-0728(88)80372-3).
- (21) Costentin, C.; Passard, G.; Robert, M.; Savéant, J. M. Ultraefficient Homogeneous Catalyst for the CO₂-to-CO Electrochemical Conversion. *Proc. Natl. Acad. Sci. USA* **2014**, *111* (42), 14990–14994. <https://doi.org/10.1073/PNAS.1416697111>
- (22) Deeba, R.; Chardon-Noblat, S.; Costentin, C. Importance of Ligand Exchange in the Modulation of Molecular Catalysis: Mechanism of the Electrochemical Reduction of Nitrous Oxide with Rhenium Bipyridyl Carbonyl Complexes. <https://doi.org/10.1021/acscatal.3c01495>.
- (23) Lexa, D.; Momenteau, M.; Mispelter, J. Characterization of the Reduction Steps of Fe(III) Porphyrins. *BBA - General Subjects* **1974**, *338* (1), 151–163. [https://doi.org/10.1016/0304-4165\(74\)90344-4](https://doi.org/10.1016/0304-4165(74)90344-4).
- (24) Römel, C.; Song, J.; Tarrago, M.; Rees, J. A.; Van Gastel, M.; Weyhermüller, T.; Debeer, S.; Bill, E.; Neese, F.; Ye, S. Electronic Structure of a Formal Iron(0) Porphyrin Complex Relevant to CO₂ Reduction. *Inorg. Chem.* **2017**, *56* (8), 4745–4750. <https://doi.org/10.1021/acs.inorgchem.7b00401>.
- (25) Ceballos, B. M.; Yang, J. Y. Directing the Reactivity of Metal Hydrides for Selective CO₂ Reduction. *Proc. Natl. Acad. Sci. USA* **2018**, *115* (50), 12686–12691. <https://doi.org/10.1073/PNAS.1811396115>.
- (26) Costentin, C.; Robert, M.; Saveant, J.-M. Current Issues in Molecular Catalysis Illustrated by Iron Porphyrins as Catalysts of the CO₂-to-CO Electrochemical Conversion. *Acc. Chem. Res.* **2015**, *48*, 2996–3006.

- (27) Cunningham, D. W.; Yang, J. Y. Kinetic and Mechanistic Analysis of a Synthetic Reversible CO₂/HCO₂ Electrocatalyst. *Chem. Commun.* **2020**, *56*, 12965–12968. <https://doi.org/10.1039/d0cc055556>.
- (28) Savéant, J. M. *Elements of Molecular and Biomolecular Electrochemistry: An Electrochemical Approach to Electron Transfer Chemistry* **2006**, 1–485. <https://doi.org/10.1002/0471758078>.
- (29) Evans, D.; Ripin, D. *Evans pKa Table*.
- (30) Gilli, P.; Pretto, L.; Bertolasi, V.; Gilli, G. Predicting Hydrogen-Bond Strengths from Acid-Base Molecular Properties. The PKa Slide Rule: Toward the Solution of a Long-Lasting Problem. *Acc. Chem. Res.* **2009**, *42* (1), 33–44. <https://doi.org/10.1021/ar800001k>.
- (31) Costentin, C.; Robert, M.; Saveant, J.-M.; Tard, C. Breaking Bonds with Electrons and Protons. Models and Examples. *Acc. Chem. Res.* **2014**, *47* (1), 271–280. <https://doi.org/10.1021/ar4001444>.